ChemComm

COMMUNICATION

View Article Online
View Journal | View Issue

Check for updates

Cite this: *Chem. Commun.*, 2020, **56**, 6660

Received 13th April 2020,
Accepted 3rd May 2020

DOI: 10.1039/d0cc02658a

rsc.li/chemcomm

Published on 04 May 2020. Downloaded by Wuhan University on 7/28/2021 10:27:12 AM.

Enhancement of long-lived luminescence in nanophosphors by surface defect passivation†

Linna Fu,‡[a] Jie Wang, ‡[ab] Na Chen,[b] Qinqin Ma,[b] Danqing Lu[c] and Quan Yuan *[ab]

Herein, we found that surface defects quench persistent luminescence in nanophosphors. Passivation of surface defects by thermal treatment or surface coating can effectively enhance the intensity and prolong the decay time of persistent luminescence. The surface passivated persistent nanophosphors are promising in autofluorescence-free bioimaging and time-gated steganography.

Persistent luminescence (PersL) is an optical phenomenon whereby afterglow remains for seconds or even months after the stoppage of excitation.[1,2] With their unique luminescence properties, persistent phosphors have long been used in areas including security signs, traffic signage dials, and decoration.[3] In the past few years, with the development of persistent luminescent nanoparticles (PLNPs), the application of persistent phosphors has been extended to biosensing,[4–6] bioimaging,[7–11] and cancer treatment.[12–19] In biosensing/bioimaging, PLNPs can eliminate autofluorescence and light-scattering interference by collecting PersL signals after removing the excitation, leading to a significantly improved signal-to-background ratio and sensitivity.[4,10] As for cancer treatment, particularly in photodynamic therapy,[18,19] the excitation energy can be trapped by PLNPs and slowly released to activate photosensitizers after the excitation ceases. In this way, a single dose of excitation can continuously generate reactive oxygen species for cancer treatment, minimizing the tissue damage associated with continuous irradiation. PLNPs hold great potential in biosensing, bioimaging and cancer treatment.

It is generally accepted that PersL originates from the crystal defects in phosphors.[20–22] Defects refer to the irregular arrangement of atoms in the crystal, such as vacancies and interstitials.[23] Upon excitation, charge carriers are generated in persistent phosphors, and the charge carriers can be trapped by the defects. Under thermal or optical stimulation, the trapped charge carriers can get out of the defects and further recombine to generate the PersL.[24] Researchers have shown that PersL can be enhanced with increased amounts of defects in the phosphors, while a high density of defects will quench the PersL due to the concentration quenching effect.[25] Although much effort has been made in studying the relationships between crystal defects and PersL, the effects of surface defects on PersL in persistent phosphors, particularly in PLNPs, remains largely unexplored. Surface defects are produced for the balance of charge due to the abundantly exposed atoms on the nanoparticle surface.[26–28] Surface defects widely exist on PLNPs and influence the luminescence properties of PLNPs. Studying how surface defects regulate PersL can contribute to the research on the PersL mechanism and provide valuable instruction for optimizing the performance of PLNPs in biomedical applications.

Herein, we show that surface defects quench PersL in PLNPs. Passivation of the PLNPs surface can effectively enhance the intensity of PersL and prolong the decay time. Zinc gallogermanate PLNPs with near-IR emission were used as the model in this study. Thermal treatment and surface coating were employed to passivate the surface defects on ZGGO:Cr PLNPs (Scheme 1). The thermally treated ZGGO:Cr PLNPs and surface coated ZGGO:Cr PLNPs all show enhanced PersL intensity and increased decay time compared to the untreated ZGGO:Cr. We further investigated the applications of the surface passivated ZGGO:Cr PLNPs in autofluorescence-free bioimaging and time-gated anticounterfeiting. The surface passivated ZGGO:Cr PLNPs display a much higher signal-to-background ratio and sensitivity than the untreated ZGGO:Cr PLNPs in *in vivo* imaging. Furthermore, the surface passivated ZGGO:Cr PLNPs can serve as time-gated invisible ink for steganography due to their long-lived luminescence. Our work may shed new light on the relationships between crystal defects and PersL, and may provide valuable instructions for the design of PLNPs with bright PersL for biomedical and informatics applications.

[a] *Institute of Chemical Biology and Nanomedicine, State Key Laboratory of Chemo/Biosensing and Chemometrics, College of Chemistry and Chemical Engineering, Hunan University, Changsha 410082, China. E-mail: yuanquan@whu.edu.cn*
[b] *Key Laboratory of Analytical Chemistry for Biology and Medicine (Ministry of Education), College of Chemistry and Molecular Sciences, Wuhan University, Wuhan 430072, China*
[c] *School of Science, Central South University of Forestry and Technology, Changsha 410004, China*

† Electronic supplementary information (ESI) available. See DOI: 10.1039/d0cc02658a

‡ These authors contributed equally to this work.

This journal is © The Royal Society of Chemistry 2020

Published on 04 May 2020. Downloaded by Wuhan University on 7/28/2021 10:27:12 AM.

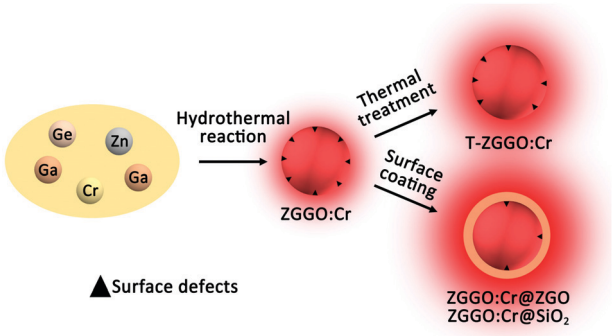

Scheme 1 Overview of surface defect passivation of PLNPs by thermal treatment and surface coating.

The zinc gallogermanate ($Zn_{1.2}Ga_{1.6}Ge_{0.2}O_4$:Cr, ZGGO:Cr) PLNPs were synthesized through a hydrothermal protocol.[26] Thermal treatment[29] was used for surface passivation of the ZGGO:Cr PLNPs. Fig. 1a and b show that both ZGGO:Cr and the thermally treated ZGGO:Cr (T-ZGGO:Cr) PLNPs are well-dispersed. Meanwhile, the morphology and size of the PLNPs are uniform. High-resolution transmission electron microscopy (HRTEM) images of ZGGO:Cr and T-ZGGO:Cr PLNPs (inset in Fig. 1a and b) show clear lattice fringes, revealing that ZGGO:Cr and T-ZGGO:Cr PLNPs are highly crystallized. The size distribution analysis suggests that thermal treatment does not influence the size of the ZGGO:Cr PLNPs (Fig. 1c and Table S1, ESI†). Both ZGGO:Cr and T-ZGGO:Cr PLNPs have an average diameter of around 13 nm.

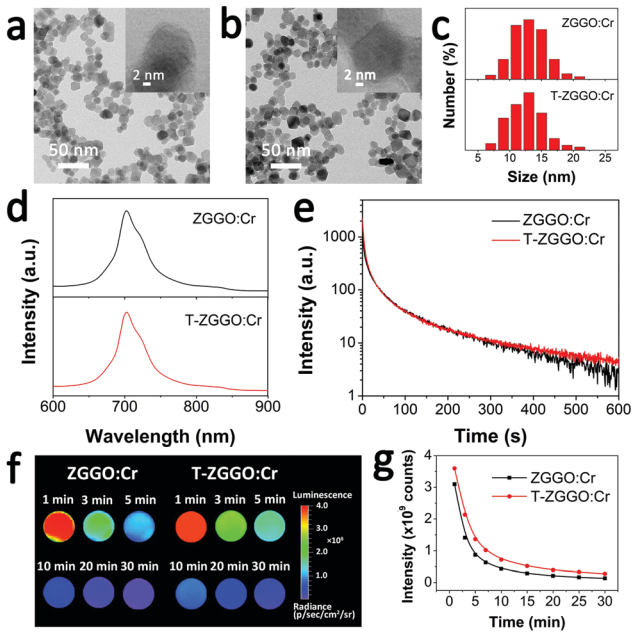

Fig. 1 (a) TEM and HRTEM images of untreated ZGGO:Cr PLNPs. (b) TEM and HRTEM images of T-ZGGO:Cr PLNPs. (c) Corresponding size distributions of untreated ZGGO:Cr PLNPs and T-ZGGO:Cr PLNPs. The photoluminescence spectra (d) and PersL decay curves (e) of ZGGO:Cr and T-ZGGO:Cr PLNPs. (f) PersL decay images of ZGGO:Cr and T-ZGGO:Cr PLNPs. (g) PersL intensity of ZGGO:Cr and T-ZGGO:Cr PLNPs *vs.* time.

The luminescence properties of the ZGGO:Cr and T-ZGGO:Cr PLNPs were further studied. As shown in Fig. 1d, the emission peak at around 700 nm is attributed to the $^2E \rightarrow {}^4A_2$ emission of Cr^{3+}.[3] The luminescence decay curves in Fig. 1e show that T-ZGGO:Cr PLNPs possess stronger PersL intensity than the ZGGO:Cr PLNPs. The PersL properties of ZGGO:Cr and T-ZGGO:Cr PLNPs were further mapped with an IVIS imaging system. Both PLNPs display PersL that remains for over 30 min, however a stronger PersL intensity from T-ZGGO:Cr PLNPs is observed (Fig. 1f). The luminescence intensity shown in Fig. 1f was quantified and is presented in Fig. 1g, clearly showing stronger PersL in T-ZGGO:Cr PLNPs. The thermoluminescence (TL) in ZGGO:Cr and T-ZGGO:Cr PLNPs was further measured (Fig. S7, ESI†). An obvious enhancement of TL intensity at around 130 °C was observed. The TL peaks in the region of 50–150 °C are the main sources of PersL.[30,31] Thus, the enhanced TL again indicates the increased PersL intensity in T-ZGGO:Cr PLNPs. Previous studies have shown that an amorphous phase existed on the surface of nanoparticles, where the surface defects quench the luminescence of nanophosphors. Thermal treatment can improve the surface crystallization of nanoparticles and passivate the surface defects.[29,32] Therefore, we reason that thermal treatment can promote the crystallization of the amorphous phase on ZGGO:Cr PLNPs, leading to the passivation of surface defects and the enhancement of PersL.[30]

To further confirm the phenomenon that surface defect passivation can enhance PersL in PLNPs, the classic surface coating method[28,29] was employed to passivate the surface defects on ZGGO:Cr PLNPs. Specifically, core–shell structured $Zn_{1.2}Ga_{1.6}Ge_{0.2}O_4$:Cr@$ZnGaO_4$ (ZGGO:Cr@ZGO) and $Zn_{1.2}Ga_{1.6}Ge_{0.2}O_4$:Cr@$SiO_2$ (ZGGO:Cr@SiO_2) PLNPs were prepared.[33] The TEM images (Fig. 2a and Fig. S8, ESI†) show that the as-synthesized ZGGO:Cr@ZGO PLNPs display a uniform quasi-spherical shape. The average diameter of the ZGGO:Cr@ZGO PLNPs is about 15 nm. A high-angle annular dark-field scanning transmission electron microscopy (HAADF-STEM) image (Fig. 2a) clearly shows the core–shell structure of the ZGGO:Cr@ZGO PLNPs.[25] Regarding the ZGGO:Cr@SiO_2 PLNPs, a uniform quasi-spherical shape and good dispersibility of the PLNPs are observed (Fig. 2b and Fig. S9, ESI†). The average diameter of the ZGGO:Cr@SiO_2 PLNPs was determined to be about 18 nm. Moreover, the HRTEM image shows the well-defined core–shell structure of the ZGGO:Cr@SiO_2 PLNPs.

The luminescence properties of ZGGO:Cr@ZGO and ZGGO:Cr@SiO_2 PLNPs were further investigated. The emission bands of ZGGO:Cr@ZGO and ZGGO:Cr@SiO_2 PLNPs peak at around 700 nm (Fig. S13 and S14, ESI†). The luminescence decay curves in Fig. 2c show that ZGGO:Cr@ZGO and ZGGO:Cr@SiO_2 PLNPs possess stronger PersL intensity than that of ZGGO:Cr. The PersL images mapped by an IVIS imaging system further demonstrate that ZGGO:Cr@ZGO and ZGGO:Cr@SiO_2 PLNPs have much stronger PersL intensity and prolonged decay time than those of the untreated ZGGO:Cr (Fig. 2d and e). Previous studies showed that surface coating can passivate the defects on core nanoparticles by means including filling the surface vacancies, leading to an improvement in luminescence quantum

Published on 04 May 2020. Downloaded by Wuhan University on 7/28/2021 10:27:12 AM.

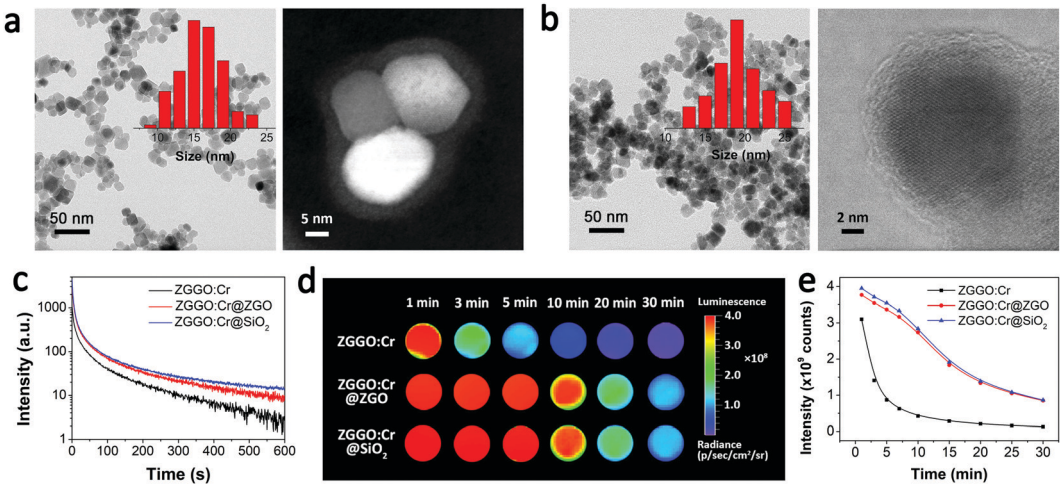

Fig. 2 (a) TEM image, size distribution and HAADF-STEM image of the ZGGO:Cr@ZGO PLNPs. (b) TEM image, size distribution and HRTEM image of the ZGGO:Cr@SiO_2 PLNPs. The PersL decay curves (c) and PersL decay images (d) of ZGGO:Cr, ZGGO:Cr@ZGO and ZGGO:Cr@SiO_2 PLNPs. (e) PersL intensity of ZGGO:Cr, ZGGO:Cr@ZGO and ZGGO:Cr@SiO_2 PLNPs *vs.* time.

yields in nanophosphors.[25,27] Thus, the enhanced PersL in ZGGO:Cr@ZGO and ZGGO:Cr@SiO_2 PLNPs can be attributed to the passivation of surface defects on the ZGGO:Cr core by surface coating. Collectively, the above results clearly show that surface coating can efficiently enhance the PersL intensity and prolong the decay time in PLNPs by passivating surface defects.

It is noteworthy that surface coating is more efficient in enhancing the PersL in PLNPs compared with thermal treatment (Fig. 1e–g and 2c–e). In the T-ZGGO:Cr PLNPs, a large amount of surface defects still existed due to the abundantly exposed atoms on the nanoparticle surface, whereas in the ZGGO:Cr@ZGO and ZGGO:Cr@SiO_2 PLNPs, the ZGGO:Cr core is well wrapped by the shell layer, significantly reducing the surface exposed atoms on the ZGGO:Cr core. Therefore, the outstanding performance of surface coating in enhancing the PersL in PLNPs can be attributed to its strong ability to passivate surface defects. It is also worth noting that the PersL enhancement performance of the SiO_2 shell is better than that of the ZGO shell (Fig. 2c–e). Previous studies have shown that the luminescence enhancement performance of the shell layer increases with the increasing thickness of the shell.[34,35] The thickness of the SiO_2 shell in ZGGO:Cr@SiO_2 PLNPs is about 2.5 nm, much larger than that of the ZGO shell ($\sim$1.0 nm) in ZGGO:Cr@ZGO PLNPs. As a result, the SiO_2 shell is better than the ZGO shell in enhancing PersL in our study.

The potential applications of the surface passivated PLNPs in autofluorescence-free bioimaging were further investigated. The PLNPs were subcutaneously injected into mice, and the mouse carrying PLNPs showed strong tissue autofluorescence under excitation. After excitation ceases, the autofluorescence disappears, whereas the PersL signal of the PLNPs remains, making it possible to eliminate the autofluorescence interference and improve the imaging sensitivity (Fig. 3a). A rhodamine B dye was adopted for comparison in this study. As shown in the left panel of Fig. 3b, the rhodamine B injected mouse showed strong autofluorescence under *in situ* excitation, and the fluorescence

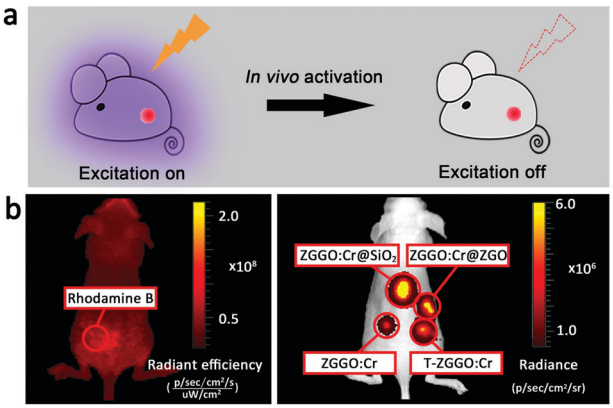

Fig. 3 (a) Schematic illustration of eliminating tissue autofluorescence interference with PLNPs. (b) *In vivo* imaging with rhodamine B, ZGGO:Cr, T-ZGGO:Cr, ZGGO:Cr@ZGO and ZGGO:Cr@SiO_2 PLNPs.

signal from rhodamine B was completely buried by the autofluorescence. However, a strong luminescence signal from the mouse without any autofluorescence interference can be obtained (right panel) by collecting emission signals from PLNPs after autofluorescence disappears, clearly showing that the PLNPs show much higher sensitivity than rhodamine B in bioimaging. Moreover, compared with the ZGGO:Cr PLNPs, the PersL signals from the T-ZGGO:Cr, ZGGO:Cr@ZGO and ZGGO:Cr@SiO_2 PLNPs are much stronger, indicating that surface passivation can efficiently enhance PersL intensity and increase the imaging sensitivity of PLNPs. These results clearly show the potent ability of surface passivation in improving the bioimaging sensitivity of PLNPs.

The potential applications of the surface passivated PLNPs in time-gated steganography were further investigated, as illustrated in Fig. 4a. The designed code information is printed by a commercial inkjet printer with cartridges containing ZGGO:Cr@ZGO PLNPs ink and a commercial red UV ink. Under UV lamp excitation, a false code "888" (Fig. 4b, left panel) is observed,

 This journal is © The Royal Society of Chemistry 2020

Published on 04 May 2020. Downloaded by Wuhan University on 7/28/2021 10:27:12 AM.

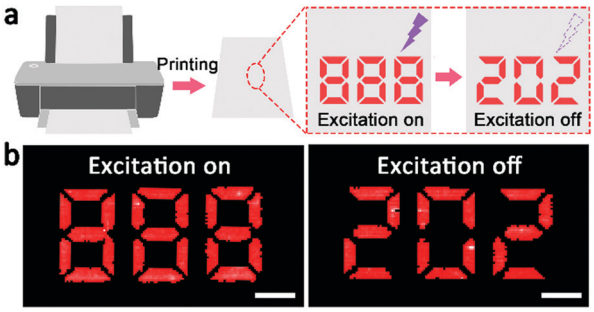

Fig. 4 (a) Schematic illustration of the anticounterfeiting strategy on office paper based on surface coated ZGGO:Cr@ZGO ink. (b) Images of the false code "888" under excitation and the correct code "202" after the stoppage of excitation. The code is shown in false colour. Scale bar = 2 cm.

whereas after excitation ceases, the correct code "202" (Fig. 4b, right panel) appears. The above images demonstrate that ZGGO:Cr@ZGO PLNPs are promising in the application of steganography with their bright PersL.

In this work, we have shown that surface defects quench the PersL in PLNPs. Passivating surface defects on PLNPs can enhance the PersL intensity and prolong decay time. Thermal treatment and surface coating are efficient ways to passivate the surface defects on PLNPs. Besides, surface coating is more efficient to passivate surface defects. With the improved PersL properties, the PLNPs are promising for applications in autofluorescence-free bioimaging and time-gated steganography. Our work provides new insight into understanding the mechanism of PersL and can give inspiration for the design of PLNPs in emerging applications.

This work was supported by the National Natural Science Foundation of China (21925401 and 21904100) and Changsha Municipal Science and Technology Projects, China (kq1901030).

Conflicts of interest

There are no conflicts to declare.

Notes and references

1 L. Liang, N. Chen, Y. Y. Jia, Q. Q. Ma, J. Wang, Q. Yuan and W. H. Tan, *Nano Res.*, 2019, **12**, 1279–1292.
2 Q. S. Lin, Z. H. Li and Q. Yuan, *Chin. Chem. Lett.*, 2019, **30**, 1547–1556.
3 Z. W. Pan, Y. Y. Lu and F. Liu, *Nat. Mater.*, 2012, **11**, 58–63.
4 J. Wang, Q. Q. Ma, W. Zheng, H. Y. Liu, C. Q. Yin, F. B. Wang, X. Y. Chen, Q. Yuan and W. H. Tan, *ACS Nano*, 2017, **11**, 8185–8191.
5 Z. H. Zhou, W. Zheng, J. T. Kong, Y. Liu, P. Huang, S. Y. Zhou, Z. Chen, J. L. Shi and X. Y. Chen, *Nanoscale*, 2017, **9**, 6846–6853.
6 F. X. Su, X. Zhao, C. Dai, Y. J. Li, C. X. Yang and X. P. Yan, *Chem. Commun.*, 2019, **55**, 5283–5286.
7 X. H. Lin, L. Song, S. Chen, X. F. Chen, J. J. Wei, J. Y. Li, G. M. Huang and H. H. Yang, *ACS Appl. Mater. Interfaces*, 2017, **9**, 41181–41187.
8 Z. Z. Chen, L. C. Wang, D. Manoharan, C. L. Lee, L. C. Wu, W. T. Huang, E. Y. Huang, C. H. Su, H. S. Sheu and C. S. Yeh, *Adv. Mater.*, 2019, **31**, 1905087.
9 L. D. Hu, Y. Fan, L. Liu, X. M. Li, B. Z. Zhao, R. Wang, P. Y. Wang, A. M. El-Toni and F. Zhang, *Adv. Opt. Mater.*, 2017, **5**, 1700680.
10 T. Maldiney, A. Bessière, J. Seguin, E. Teston, S. K. Sharma, B. Viana, A. J. Bos, P. Dorenbos, M. Bessodes, D. Gourier, D. Scherman and C. Richard, *Nat. Mater.*, 2014, **13**, 418–426.
11 E. Teston, T. Maldiney, I. Marangon, J. Volatron, Y. Lalatonne, L. Motte, C. Boisson-Vidal, G. Autret, O. Clément, D. Scherman, F. Gazeau and C. Richard, *Small*, 2018, **14**, 1800020.
12 H. H. Liu, F. Ren, X. G. Zhou, C. Q. Ma, T. T. Wang, H. Zhang, Q. Sun and Z. Li, *Anal. Chem.*, 2019, **91**, 15064–15072.
13 Y. J. Li, C. X. Yang and X. P. Yan, *Anal. Chem.*, 2018, **90**, 4188–4195.
14 W. P. Fan, N. Lu, C. Xu, Y. J. Liu, J. Lin, S. Wang, Z. Y. Shen, Z. Yang, J. L. Qu, T. F. Wang, S. P. Chen, P. Huang and X. Y. Chen, *ACS Nano*, 2017, **11**, 5864–5872.
15 J. Wang, J. L. Li, J. N. Yu, H. W. Zhang and B. B. Zhang, *ACS Nano*, 2018, **12**, 4246–4258.
16 J. H. Liu, T. Lécuyer, J. Séguin, N. Mignet, D. Scherman, B. Viana and C. Richard, *Adv. Drug Delivery Rev.*, 2019, **138**, 193–210.
17 S. Q. Wu, C. X. Yang and X. P. Yan, *Adv. Funct. Mater.*, 2017, **27**, 1604992.
18 L. Song, P. P. Li, W. Yang, X. H. Lin, H. Liang, X. F. Chen, G. Liu, J. Li and H. H. Yang, *Adv. Funct. Mater.*, 2018, **28**, 1707496.
19 G. Y. Liu, S. H. Zhang, Y. H. Shi, X. Y. Huang, Y. Y. Tang, P. Chen, W. L. Si, W. Huang and X. C. Dong, *Adv. Funct. Mater.*, 2018, **28**, 1804317.
20 Y. Li, M. Gecevicius and J. R. Qiu, *Chem. Soc. Rev.*, 2016, **45**, 2090–2136.
21 B. L. Huang, *Inorg. Chem.*, 2015, **54**, 11423–11440.
22 B. L. Huang, *Phys. Chem. Chem. Phys.*, 2016, **18**, 25946–25974.
23 E. G. Seebauer and K. W. Noh, *Mater. Sci. Eng., R*, 2010, **70**, 151–168.
24 J. Wang, Q. Q. Ma, Y. Q. Wang, H. J. Shen and Q. Yuan, *Nanoscale*, 2017, **9**, 6204–6218.
25 J. Wang, Q. Q. Ma, X. X. Hu, H. Y. Liu, W. Zheng, X. Y. Chen, Q. Yuan and W. H. Tan, *ACS Nano*, 2017, **11**, 8010–8017.
26 W. Zhou and H. G. Fu, *Inorg. Chem. Front.*, 2018, **5**, 1240–1254.
27 F. Wang, J. Wang and X. G. Liu, *Angew. Chem., Int. Ed.*, 2010, **49**, 7456–7460.
28 Q. Q. Su, S. Y. Han, X. J. Xie, H. M. Zhu, H. Y. Chen, C. K. Chen, R. S. Liu, X. Y. Chen, F. Wang and X. G. Liu, *J. Am. Chem. Soc.*, 2012, **134**, 20849–20857.
29 W. J. Bian, Y. Lin, T. Wang, X. Yu, J. B. Qiu, M. Zhou, H. M. Luo, S. F. Yu and X. H. Xu, *ACS Nano*, 2018, **12**, 3623–3628.
30 Y. Li, B. H. Li, C. C. Ni, S. X. Yuan, J. Wang, Q. Tang and Q. Su, *Chem. – Asian J.*, 2014, **9**, 494–499.
31 H. F. Wang, X. Chen, F. Feng, X. Ji and Y. Zhang, *Chem. Sci.*, 2018, **9**, 8923–8929.
32 Q. H. Min, J. Lei, X. Guo, T. Wang, Q. H. Yang, D. C. Zhou, X. Yu, S. F. Yu, J. B. Qiu, Q. Q. Zhan and X. H. Xu, *Adv. Funct. Mater.*, 2020, **30**, 1906137.
33 Y. H. Deng, Y. Cai, Z. K. Sun, J. Liu, C. Liu, J. Wei, W. Li, C. Liu, Y. Wang and D. Y. Zhao, *J. Am. Chem. Soc.*, 2010, **132**, 8466–8473.
34 Y. Fan, P. Y. Wang, Y. Q. Lu, R. Wang, L. Zhou, X. L. Zheng, X. M. Li, J. A. Piper and F. Zhang, *Nat. Nanotechnol.*, 2018, **13**, 941–946.
35 P. Huang, W. Zheng, S. Y. Zhou, D. T. Tu, Z. Chen, H. M. Zhu, R. F. Li, E. Ma, M. D. Huang and X. Y. Chen, *Angew. Chem., Int. Ed.*, 2014, **53**, 1252–1257.